

Article

CeO₂-Based Two-Dimensional Layered Nanocomposites Derived from a Metal–Organic Framework for Selective Electrochemical Dopamine Sensors

Chengjie Ge ¹, Rajendran Ramachandran ^{1,2} and Fei Wang ^{1,3,*} 

¹ School of Microelectronics, Southern University of Science and Technology, Shenzhen 518055, China; 11712522@mail.sustech.edu.cn (C.G.); ramachandran@sustech.edu.cn (R.R.)

² SUSTech Academy for Advanced Interdisciplinary Studies, Southern University of Science and Technology, Shenzhen 518055, China

³ Engineering Research Center of Integrated Circuits for Next-Generation Communications, Ministry of Education, Shenzhen 518055, China

* Correspondence: wangf@sustech.edu.cn

Received: 12 July 2020; Accepted: 24 August 2020; Published: 28 August 2020



Abstract: In this work, we demonstrate the incorporation of two-dimensional (2D) layered materials into a metal–organic framework (MOF) derived from one-dimensional (1D) cerium oxide (CeO₂) for the electrochemical detection of dopamine. Ce-MOF was employed as a sacrificial template for preparing CeO₂ with 2D materials by the pyrolysis process. The influence of the pyrolysis temperature was studied to achieve a better crystal structure of CeO₂. Siloxene improved the dopamine sensing performance of CeO₂ compared with graphitic carbon nitride (g-C₃N₄) due to the basal plane surface oxygen and hydroxyl groups of 2D siloxene. Under optimal conditions, the fabricated CeO₂/siloxene electrode exhibited a detection limit of 0.292 μM, with a linear range from 0.292 μM to 7.8 μM. This work provides a novel scheme for designing the CeO₂ material with siloxene for excellent dopamine sensors, which could be extended towards other biosensing applications.

Keywords: differential pulse voltammetry; dopamine; CeO₂; siloxene

1. Introduction

Dopamine (DA) is one of the most abundant catecholamine neurotransmitters, playing a crucial role in the human brain [1,2]. Abnormal dopamine content causes a few diseases, like brain aging, Parkinson’s syndrome, and schizophrenia. Thus, the detection of DA molecules in the central nervous system is becoming a necessary and significant task in the biosensor field [3,4]. Till now, many methods have been used to detect dopamine molecules, such as spectrophotometry, titrimetry, the chemiluminescence method, and the electrochemical method. Among these, the electrochemical detection method offers high sensitivity, low cost, and excellent selectivity. Hence, the electrochemical detection of DA has been considered to be effective for practical usage [5–10].

On the other hand, metal–organic frameworks (MOFs) and their derived composites have drawn much interest in various applications, such as energy storage, conversion, catalysis, separation, and gas sensors, thanks to their superior material properties like a large surface area, a tunable structure, and high thermal and chemical stability [11–15]. Additionally, an MOF has been employed as a flexible template to prepare porous metal oxides/sulfides and carbon materials using the direct pyrolysis process [16–19]. Up to now, various metal oxides such as Co₃O₄, CuO, cerium oxide (CeO₂), and NiO

have been synthesized using MOFs as their sacrificial template and applied in various electrochemical applications, such as supercapacitors, batteries, and biosensors [20–23].

Among them, CeO_2 is a rare earth metal oxide that has attracted much interest in biomolecules detection due to its facile oxygen vacancy formation properties, excellent biocompatibility, and natural abundance. Furthermore, the stable redox behavior between Ce^{3+} and Ce^{4+} enhances the electrocatalytic properties of CeO_2 . Nevertheless, attaining highly electrocatalytic and selective CeO_2 for DA detection is a challenging task, as a result of its poor electrical conductivity [24–26]. Therefore, for high sensitivity and selectivity it could be an effective strategy to combine two-dimensional (2D) conductive materials with CeO_2 .

Emerging two-dimensional materials such as siloxene and graphitic carbon nitride ($\text{g-C}_3\text{N}_4$) have recently been used as excellent substrates for the electrochemical sensor field because of their high surface area, excellent electrical conductivity, and better redox abilities [27–31]. A large number of experiments have been performed on $\text{g-C}_3\text{N}_4$ and other two-dimensional materials combined with MOFs and metal oxides for electrochemical sensors. The 2D conductive materials can increase the rate of electron transport, resulting in high electrocatalytic activity [32–34]. Siloxene, a type of low-buckled structure, has been explored as an excellent candidate for the dopamine sensor, and the reported detection limit was $0.327 \mu\text{M}$ [27].

Taking into consideration the above factors, we successfully synthesized the 2D siloxene and $\text{g-C}_3\text{N}_4$ with CeO_2 and studied their electrocatalytic properties for DA detection. Although a few reports are available on MOF-derived CeO_2 for electrochemical applications, there has been no reported work on the combination of CeO_2 with $\text{g-C}_3\text{N}_4$ and siloxene, derived from a Ce-MOF for electrochemical dopamine sensors. This paper demonstrates the simple wet chemical and pyrolysis routes for the preparation of $\text{CeO}_2/\text{siloxene}$ and $\text{CeO}_2/\text{g-C}_3\text{N}_4$ composites from Ce-MOF materials and investigates their electrochemical sensing ability. Combining 2D siloxene and $\text{g-C}_3\text{N}_4$ can significantly enhance the electroactive sites of CeO_2 for DA detection. As a result of the synergistic effect of CeO_2 and $\text{g-C}_3\text{N}_4/\text{siloxene}$, the composites exhibited a better performance towards DA detection. Interestingly, $\text{CeO}_2/\text{siloxene}$ showed higher detection performance than $\text{CeO}_2/\text{g-C}_3\text{N}_4$, with a detection limit of $0.292 \mu\text{M}$. The strong coordination modes between the Ce atom and siloxene oxygen functional groups in the $\text{CeO}_2/\text{siloxene}$ composite are beneficial for improving the DA oxidation performance with good selectivity and stability, which can be applied in future electrochemical sensor applications.

2. Materials and Methods

2.1. Materials

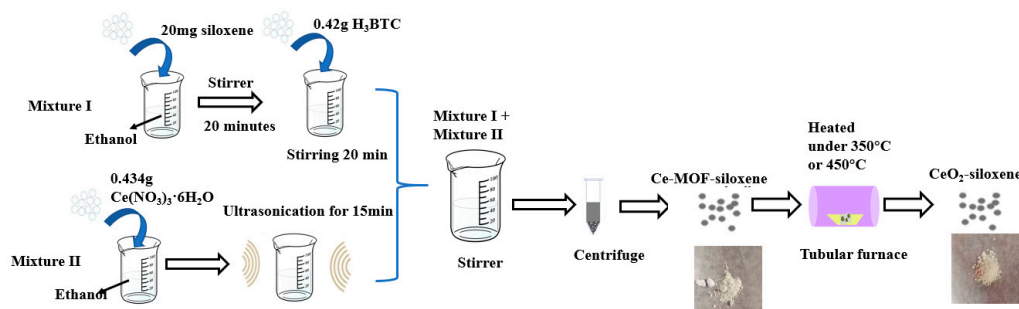
Cerium (II) nitrate hexahydrate ($\text{Ce}(\text{NO}_3)_2 \cdot 6\text{H}_2\text{O}$), 1,3,5-tricarboxylic acid (H_3BTC), urea ($\text{CH}_4\text{N}_2\text{O}$), and hydrochloric acid (HCl , 37% assay) were purchased from Sigma–Aldrich. Calcium disilicide (CaSi_2) was purchased from Alfa Aesar, China. All of the solutions were prepared using Milli-Q water (pH 7.2).

2.2. Preparation of Ce-MOF, Ce-MOF/Siloxene, and Ce-MOF/ $\text{g-C}_3\text{N}_4$ Composites

Siloxene and $\text{g-C}_3\text{N}_4$ samples were synthesized based on our previous reports [27,35]. In line with our previous report, the Ce-MOF-based composites were synthesized by a simple wet chemical route [36]. Briefly, 0.454 g of $\text{Ce}(\text{NO}_3)_2 \cdot 6\text{H}_2\text{O}$ was added into a 40 mL of water and ethanol solution (3:1 volume ratio) and stirred for 10 min (mixture I). Meanwhile, 0.494 g of H_3BTC was added into another 40 mL 25% ethanol solution and stirred for 15 min. (mixture II). Afterwards, mixture I was added drop by drop into mixture II with continuous stirring. Finally, the solid white powder was washed and centrifuged several times with ethanol and water, then dried in the vacuum oven at $80 \text{ }^\circ\text{C}$ for 12 h. The product was named Ce-MOF. Ce-MOF/siloxene and Ce-MOF/ $\text{g-C}_3\text{N}_4$ were also synthesized by a similar procedure as the abovementioned, with the addition of 20 mg of siloxene and $\text{g-C}_3\text{N}_4$ into the H_3BTC solution.

2.3. Preparation of CeO₂, CeO₂/Siloxene and CeO₂/g-C₃N₄

The bare CeO₂ and composites with siloxene and g-C₃N₄ were prepared by the pyrolysis of Ce-MOF, Ce-MOF/siloxene, and Ce-MOF/g-C₃N₄, respectively. The pyrolysis temperature was set to 350 and 450 °C for the three samples. The process of CeO₂/siloxene composite preparation is illustrated in Scheme 1.



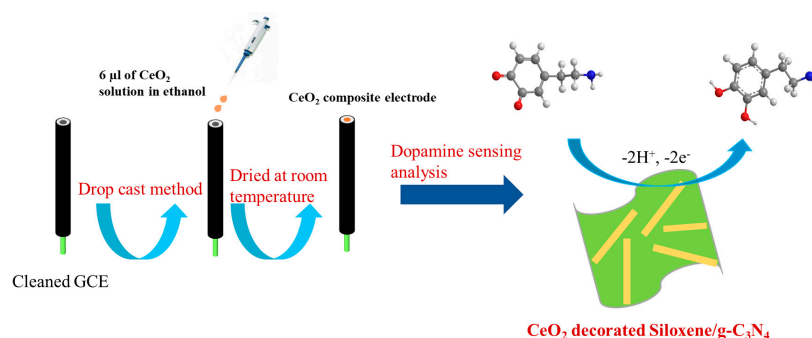
Scheme 1. Schematic diagram of cerium oxide (CeO₂)/siloxene composite preparation.

2.4. Materials Characterization

The Rigaku Smartlab diffractometer collected the powder X-ray diffraction (XRD) pattern of the prepared samples. Cu-K α radiation ($\lambda = 1.540 \text{ \AA}$) was utilized to characterize the samples with the 2θ interval from 6 to 70°. A scanning electron microscope (SEM, Zeiss Merlin, Jena, Germany) and the high-resolution transmission electron microscope (TEM, Tecnai F30, FEI Ltd., Hillsboro, OR, USA) were used to identify the samples' structural morphology. The porosity and surface area of the samples was characterized by the Brunauer–Emmett–Teller (BET, ASAP2020, Duluth, GA, USA) instrument.

2.5. Preparation of Modified Electrodes for Dopamine Detections and Electrochemical Analysis of Detections

Initially, aluminum oxide powder of 0.05 μM was used to polish a bare glassy carbon electrode (GCE). After that, the electrode was sonicated for 5 min in the deionized water and dried at room temperature. Meanwhile, 5 mg of active material (CeO₂, CeO₂/siloxene, CeO₂/g-C₃N₄) was inserted into 5 mL of ethanol solution and sonicated for 30 min. Later, 6 μL of the active material solution was coated on the polished GCE by the drop-casting method and allowed to dry at room temperature. Scheme 2 shows the fabrication of the CeO₂/siloxene- and g-C₃N₄-modified GCE electrodes and the DA sensing mechanism. Cyclic Voltammetry (CV) was used to optimize the electrodes for enhanced redox performance of DA detection. After that, the differential pulse voltammetry (DPV) technique was employed to investigate the DA detection of the modified electrode (CeO₂/siloxene/GCE) in the 0.1 M phosphate-buffered saline (PBS, pH = 7.0) solution under different concentrations of DA. The interference study in the presence of interfering compounds was carried out after washing the electrodes by the consecutive addition of various analytes to avoid the formation of contaminants. The repeatability test was carried out with a CeO₂/siloxene/GCE electrode for five consecutive runs, and the stability of the CeO₂/siloxene/GCE electrode was examined for 15 days in the presence of 1000 μL of 0.2 mM of DA-containing 0.1 M PBS solution by the DPV measurement.



Scheme 2. Electrode modification process and dopamine sensing mechanism of the modified electrode.

3. Results and Discussion

3.1. Structural and Morphological Characterization

The X-ray diffraction patterns of the Ce-MOFs composites and CeO₂ composites are shown in Figure 1. The Ce-MOF's sharp diffraction peaks are in close agreement with the XRD pattern of previously reported work [36], which confirms the better crystalline nature and phase purity of the Ce-MOF (Figure S1). After annealing, the diffraction peaks of the Ce-MOF were relocated at 28.7°, 33.1°, 47.4°, and 56.6°, corresponding to the (111), (200), (220), and (311) planes of CeO₂ cubic phase, which matched with JCPDS card no. 34-0394 (Figure 1) [37]. The disappearance of the MOF peaks and the rise of new peaks after pyrolysis confirms the effective conversion of MOF to the crystalline phase of CeO₂. The crystalline nature of CeO₂ was investigated at two pyrolysis temperatures. As shown in Figure 1, the diffraction peak intensity of CeO₂ prepared at 450 °C is higher than that of samples prepared at 350 °C, indicating better crystallinity increases in grain size. Interestingly, there is no distinct different peak among the CeO₂, CeO₂/siloxene, and CeO₂/g-C₃N₄, probably due to the excellent crystallinity of CeO₂ and the relatively low weight percentage of the siloxene and g-C₃N₄.

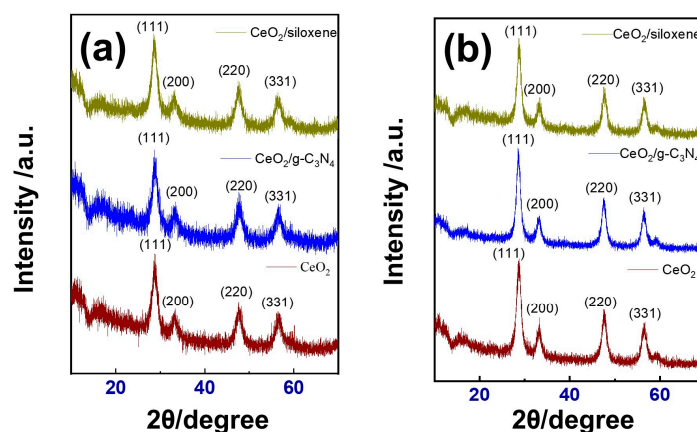


Figure 1. X-ray diffraction pattern of (a) cerium oxide (CeO₂) and composites pyrolyzed at 350 °C, and (b) CeO₂ and composites pyrolyzed at 450 °C.

The morphologies of the samples as prepared were characterized by SEM and the images of the samples are shown in Figure 2. Figure 2a,b shows the nanorod structure of the Ce-MOF with a diameter of ~150 nm and lengths of a few micrometers. After being pyrolyzed, the obtained CeO₂ retained a structure identical to that of the Ce-MOF without affecting the rod shape. Interestingly, a more extended nanorod structure was observed in the CeO₂ sample prepared at 450 °C (Figure 2d), whereas some broken structures in the rod were observed for the CeO₂ sample prepared at 350 °C (Figure 2c). The well-oriented nanorod CeO₂ structure and its composites would enhance the redox abilities of DA sensors. Figure 2e–h shows the SEM images of CeO₂/siloxene and CeO₂/g-C₃N₄ samples,

which were pyrolyzed at 350 °C and 450 °C, respectively. From these figures, the CeO₂ nanorods were uniformly distributed on the surface of the siloxene and g-C₃N₄ with a slight agglomeration of CeO₂ nanorods. Since the sensing properties of the active materials are strongly dependent on their crystalline nature and well-defined structure (as shown in Figures 1 and 2), the samples pyrolyzed at 450 °C have been used for other characterization and electrochemical measurements, as a result of their higher crystallinity behavior.

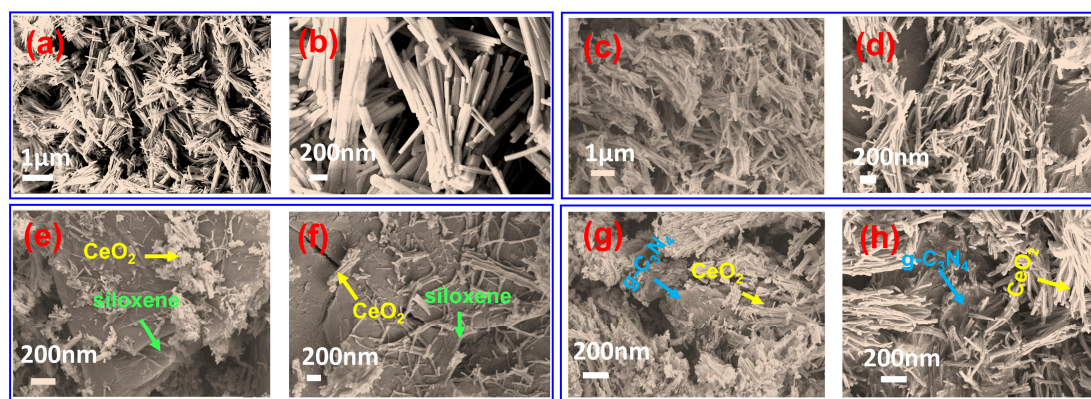


Figure 2. Scanning electron microscope (SEM) images of (a,b) Ce-MOF, pyrolyzed at 350 °C; (c) Bare CeO₂; (e) CeO₂/siloxene; (g) CeO₂/graphitic carbon nitride (g-C₃N₄), pyrolyzed at 450 °C; (d) Bare CeO₂; (f) CeO₂/siloxene; and (h) CeO₂/g-C₃N₄.

The surface area and porosity of the as-prepared CeO₂-based composites (pyrolyzed at a temperature of 450 °C) were evaluated by BET analysis, and the N₂ adsorption–desorption isotherms are shown in Figure 3a,b. As shown in Figure 3a, the isotherms of bare CeO₂ and CeO₂/siloxene and of CeO₂/g-C₃N₄ showed the type IV isotherm having a sharp hysteresis loop in the relative pressure between 0.8 and 1.0, which suggests that the samples have a mesoporous structure. The BET surface area is calculated as 95.91, 75.73, and 78.23 m² g^{−1} for CeO₂, CeO₂/siloxene, and CeO₂/g-C₃N₄, respectively. The multilayer structure of siloxene and g-C₃N₄ might be responsible for dropping the surface area of the composites. Though the surface area of the CeO₂/siloxene composite was lower than that of CeO₂/g-C₃N₄, the planner structure of the siloxene is beneficial for π – π interaction with the dopamine structure, resulting in the enhanced sensing properties. Additionally, the mesoporous feature of the CeO₂ composites was validated with a Barrett–Joyner–Halenda (BJH) analysis, as shown in Figure 3b. On the BJH curve, the samples exhibited a peak centered at around 3.7 nm, which could be the optimal pore size for electrolyte ion transportation during the electrochemical DA detection.

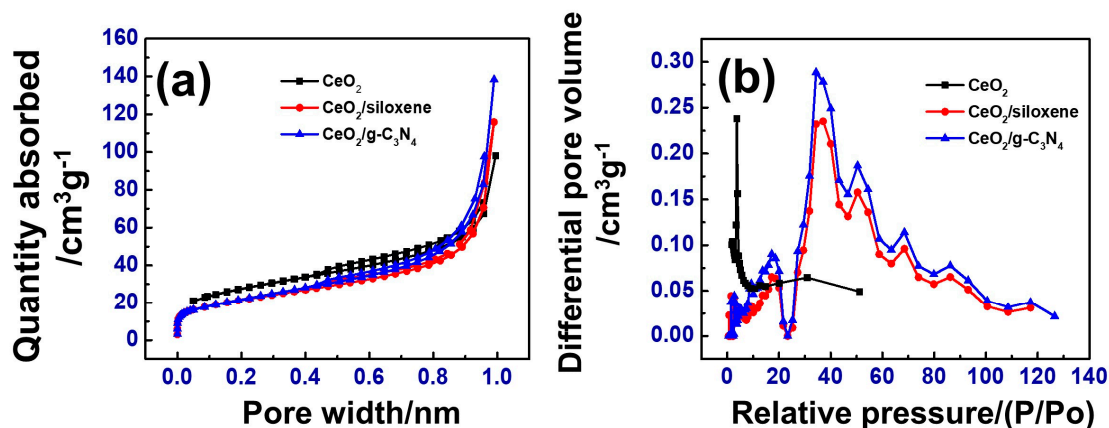


Figure 3. (a) Nitrogen adsorption–desorption isotherms; (b) Barrett–Joyner–Halenda (BJH) pore size distribution curves.

The morphology of CeO₂/siloxene was further confirmed by high-resolution transmission electron microscopy (HRTEM) analysis. As seen in Figure 4a–d, CeO₂ nanorods with uniform size (~50 nm) and lengths of a few micrometers could be observed in the CeO₂/siloxene. Additionally, the siloxene sheets were firmly anchored with the CeO₂ nanorods, which can enable faster electron transportation and active sites for DA oxidation. The HRTEM image validated the crystalline phase of CeO₂ and the amorphous nature of the siloxene sheets (Figure 4d). Energy-dispersive X-ray spectroscopy (EDS) mapping was used to confirm the presence of the Ce, Si, and O elements in the CeO₂/siloxene, and the presence of C, N, Ce, and O in the CeO₂/g-C₃N₄. The obtained results are shown in Figure 5. As shown in Figure 5, the homogenous distribution of the elements can be found throughout the samples. Additionally, the CeO₂/siloxene sample exhibited a high density of O and Si atoms distributed on the siloxene surface, which further confirms the strong coordination between the oxygen and silicon atoms in the siloxene.

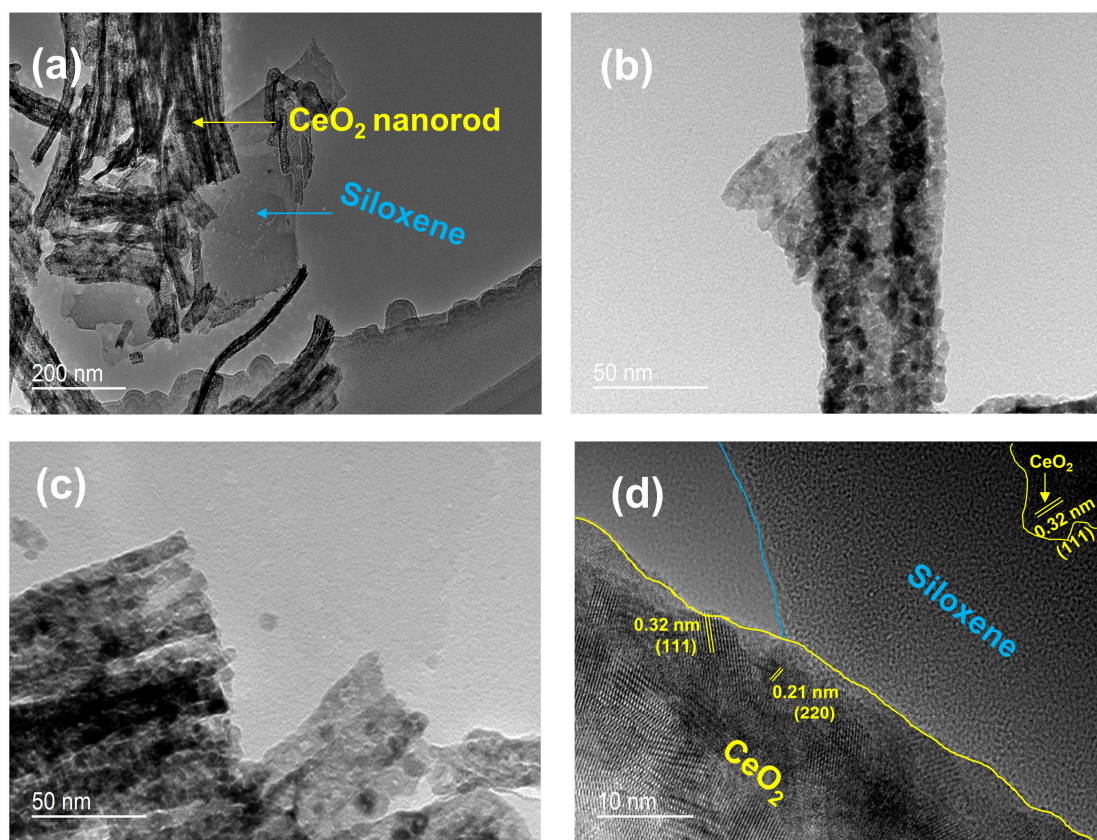


Figure 4. (a–c) Transmission electron microscopy (TEM) and (d) High-resolution transmission electron microscopy (HRTEM) images of the CeO₂/siloxene composite.

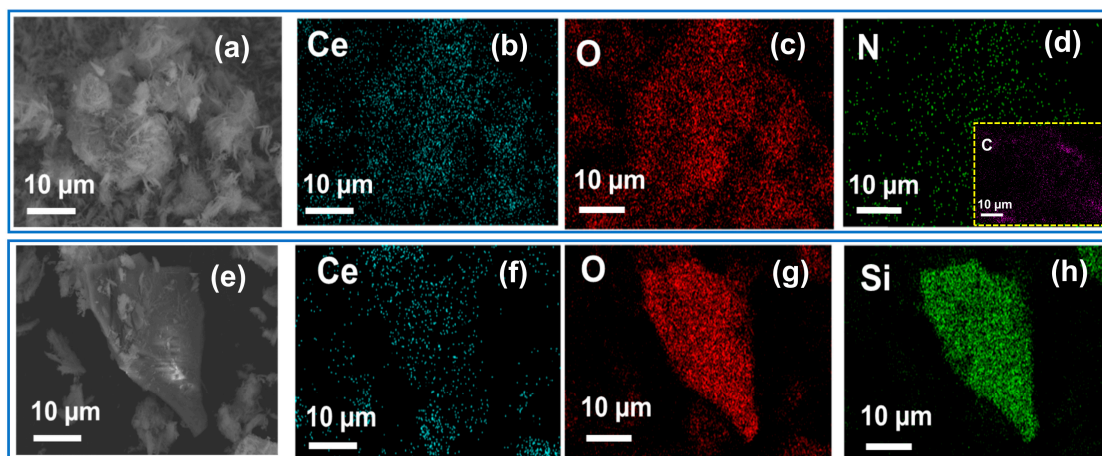


Figure 5. Energy-dispersive X-ray spectroscopy (EDS) elemental mapping of (a–d) $\text{CeO}_2/\text{g-C}_3\text{N}_4$ and (e–h) $\text{CeO}_2/\text{siloxene}$ composites.

3.2. Electrochemical Detection of Dopamine

Cyclic Voltammetry (CV) was employed to record the bare GCE and CeO_2 -, $\text{CeO}_2/\text{g-C}_3\text{N}_4$ -, and $\text{CeO}_2/\text{siloxene}$ -modified GCE electrodes' electrochemical sensing performance. A pair of redox peaks were obtained for CeO_2 and its composite-modified GCE electrodes in the presence of $0.4 \mu\text{M}$ of DA, which confirms the electrocatalytic activity of the modified electrodes for DA detection (Figure 6a). The redox peaks of the modified electrodes can be assigned to the oxidation of DA to dopaminequinone (DAQ) and the reduction of DAQ to DA [38]. The high CV current response was attributed to the larger surface area of the $\text{CeO}_2/\text{siloxene}/\text{GCE}$ electrode. It can be seen that the current response for DA oxidation is significantly enhanced for the $\text{CeO}_2/\text{siloxene}$ -modified electrode, which proves the outstanding catalytic behavior over other electrodes. The strong coordination modes between the Ce atom and siloxene oxygen functional group in $\text{CeO}_2/\text{siloxene}$ composite could improve the active sites for the DA oxidation process. From the CV results, the $\text{CeO}_2/\text{siloxene}$ -modified electrode was considered an optimal electrode for further electrochemical measurements towards DA detection.

The kinetics of the electrochemical process on the $\text{CeO}_2/\text{siloxene}$ -modified electrode surface was investigated by CV at different scan rates in the presence of $0.4 \mu\text{M}$ of DA containing 0.1 M of PBS electrolyte. As shown in Figure 6b, the oxidation and reduction peaks were shifted towards positive and negative directions upon increasing the scan rate from 20 mV s^{-1} to 200 mV s^{-1} . Additionally, the anodic and cathodic (I_{p_a} and I_{p_c}) peak currents showed an excellent linear relationship with the square root of the scan rate. They exhibited a correlation coefficient of 0.9915 and 0.9812, respectively (Figure 6c). This result confirms that DA's oxidation behavior with the $\text{CeO}_2/\text{siloxene}/\text{GCE}$ electrode is an adsorption-controlled process [39].

Since the loading amount of the active materials on the electrode can influence the current response, the CV measurements for various amounts of $\text{CeO}_2/\text{siloxene}$ loaded on the GCE electrode were carried out in $0.4 \mu\text{M}$ of DA containing 0.1 M of PBS solution. As shown in Figure S2, the intensity of the redox peak and the current response of the $6 \mu\text{L}$ coated GCE electrode reached the maximum value, which confirms the higher DA oxidation activity on the electrode/electrolyte surface. After increasing the loading amount ($8 \mu\text{L}$ and $10 \mu\text{L}$), the redox peak current decreased gradually. As per Figure 6d, the GCE electrode coated with $6 \mu\text{L}$ of $\text{CeO}_2/\text{siloxene}$ material exhibited the highest DA oxidation current response, which indicates the significant electron transportation at the electrode/electrolyte interfaces. On the other hand, excessive loading of $\text{CeO}_2/\text{siloxene}$ may lead to the formation of a thicker film with aggregated $\text{CeO}_2/\text{siloxene}$ on the GCE surface, and could hinder the DA's interaction with the electrode. Thus, electron transportation was blocked to the electrode surface due to the increase of the active material film's thickness on the GCE, resulting in a lower DA oxidation current [40,41]. From this, $6 \mu\text{L}$ of $\text{CeO}_2/\text{siloxene}$ is considered to be the optimal loading for further electrochemical analysis.

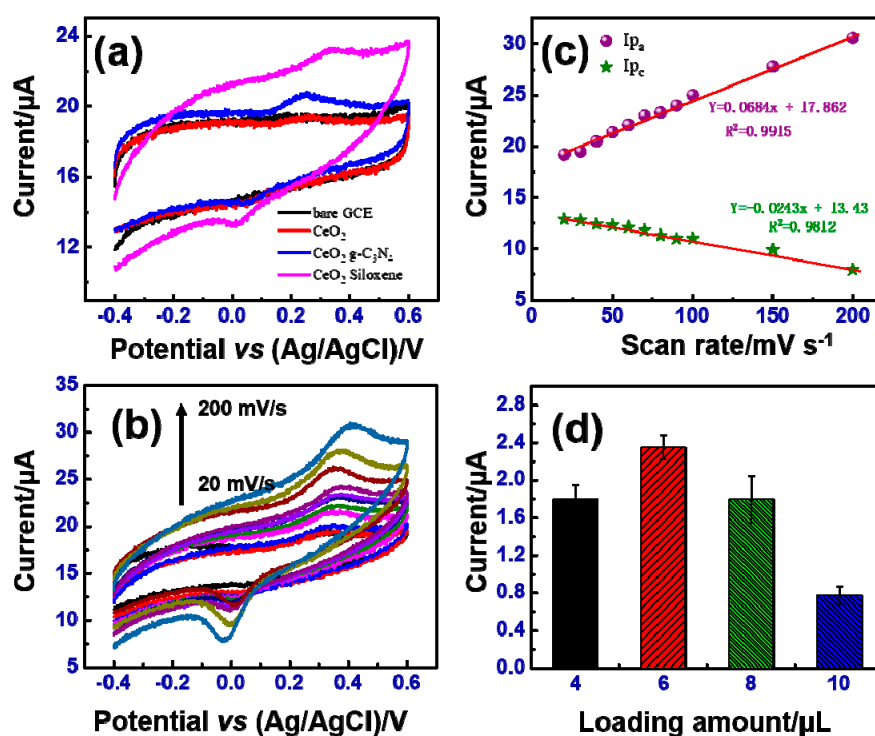


Figure 6. (a) Cyclic voltammetry response of bare glassy carbon electrodes (GCEs) and modified GCEs in $0.4 \mu\text{M}$ concentration dopamine (DA) containing 0.1 M phosphate-buffered saline (PBS) solution; (b) Cyclic voltammetry response of CeO_2 /siloxene-modified GCE electrode at different scan rates in $0.4 \mu\text{M}$ concentration DA containing 0.1 M PBS; (c) Calibration curve of the anodic and cathodic peak current versus the scan rate of the CeO_2 /siloxene-modified electrode; (d) The cyclic voltammetry peak current versus the different amounts of CeO_2 /siloxene loading.

3.3. DA Detection in the CeO_2 /Siloxene-Modified GCE Electrode

The differential pulse voltammetry technique (DPV) has several advantages: operational simplicity, high sensitivity, high accuracy, and a broad linear range for DA detection [42]. Therefore, the DPV technique was used to recognize the dopamine sensing ability of the CeO_2 /siloxene-modified electrode under the optimized conditions. Figure 7a shows the DPV response of the CeO_2 /siloxene-modified electrode at various concentrations of DA containing 0.1 M of PBS solution. From Figure 7a, it can be seen that the DA oxidation current response of the electrode gradually increased with increasing concentrations of DA (0 to $9.8 \mu\text{M}$), proving the excellent electrocatalytic behavior of the electrode for dopamine. The fabricated CeO_2 /siloxene sensor possesses a good linear range between DA concentration and the oxidation current with a correlation coefficient $R^2 = 0.9808$ (Figure 7b). Moreover, the sensor exhibited a detection limit of $0.292 \mu\text{M}$.

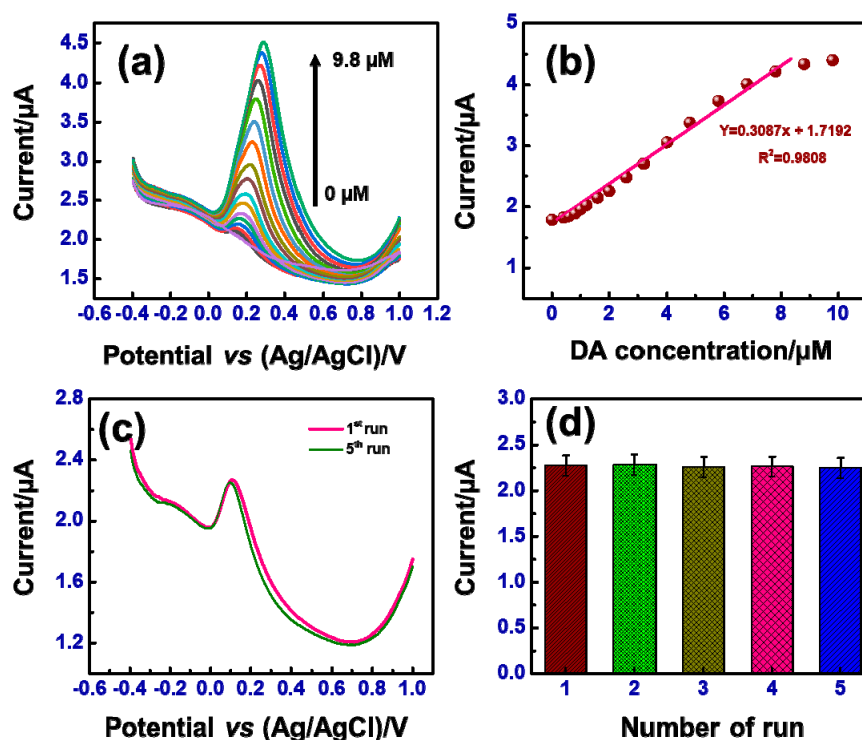


Figure 7. (a) Differential pulse voltammetry (DPV) response of the CeO₂/siloxene-modified electrode in 0.1 M PBS solution containing different concentrations of DA; (b) Linear response of the oxidation current versus DA concentrations; (c) Repeatability of a modified electrode in the presence of 1 μM of DA-containing 0.1 M PBS solution; (d) Plot of the oxidation current versus the run number for five consecutive measurements.

Table 1 shows the electrocatalytic DA sensing performance of our sensor compared with previously reported electrodes. As the table shows, the CeO₂/siloxene sensor exhibited a superior performance of DA detection, which shows a promising application in the biosensor field. The repeatability of the sensor is an essential characteristic of the electrochemical detection of DA. Figure 7c shows the DPV current response of a CeO₂/siloxene-modified electrode in 0.4 μM DA containing 0.1 M PBS solution for ten replicant measurements. The DA oxidation current response of all of the runs is almost at the same level, demonstrating the excellent repeatability of the sensing performance.

Table 1. Comparison of the analytical properties of other reported dopamine (DA) electrochemical sensors.

Electrode	Technique	Limit of Detection (μM)	Linear Range (μM)	Ref.
Beansprout/(SAM)/Au	SWV	0.478	9.9–2210	[43]
Tyrosinase/NiO/ITO	CV	1.032	2–100	[44]
P(TBA _{0.50} Th _{0.50})	EIS/CV	0.3	7.8–125	[45]
PA-MWCNT/GCE	EIS	14.1	10–1000	[46]
rGO/TiO ₂	DPV	1.5	1–35; 35–100	[47]
Ag/Graphene/GCE	LSV	5.4	10–800	[48]
CeO ₂ /siloxene/GCE	DPV	0.292	0.292–7.8	This work

Selectivity is another crucial factor in discriminating between some common species in similar analytes. Figure 8 represents an interference study of the CeO₂/siloxene-modified electrode in the presence of other interfering compounds such as ascorbic acid (AA), uric acid (UA), Adenosine

triphosphate (ATP), glucose, and rutin. As Figure 8a shows, the initial current response was observed after the addition of 1000 μL of 0.2 mM DA solution into 0.1 M PBS electrolyte. Afterwards, 1000 μL of 0.2 mM of rutin and ATP were added, and negligible changes in the oxidation current could be noticed. A remarkable change in the oxidation current was observed after the second addition of 1000 μL DA, indicating the sensor's excellent selectivity. Furthermore, the other interfering compounds (AA, UA, and glucose, 1000 μL of 0.2 mM) were also injected into the PBS solution, which revealed no fluctuations in the current and maintained the same DA oxidation current response (Figure 8b). The results prove that the CeO_2 /siloxene-modified electrode has better selectivity towards detecting DA molecules under optimal conditions. Stability is a vital characteristic for sensors; the DPV analysis was performed to investigate the stability of the CeO_2 /siloxene-modified GCE electrode. The electrode was kept in the refrigerator when not in use. As per Figure 8c, there was only a tiny change in the DA oxidation current even after 15 days compared with the initial measurement (first day). The DA oxidation current of 82.3% was maintained after two weeks of measurements, which indicates the good stability of the modified electrode for the DA sensor. Additionally, the sensor's recovery was investigated by the DPV technique before and after washing the electrodes in the PBS solution and DA containing the PBS solution. As per Figure 9a,b, the CeO_2 /siloxene-modified electrode possessed an excellent recovery characteristic in the PBS solution after washing the electrodes. However, a tiny change in the current response was observed after washing the electrode (washed 2 and washed 3 in Figure 9b) compared with the initial measurement (blank) in the PBS solution, suggesting the formation of a small quantity of contaminants on the electrode surface. Although a small difference was noticed after washing the electrodes, it was negligible compared to the DA oxidation current. These results demonstrate that one-dimensional (1D) CeO_2 nanorods with 2D siloxene sheets could be employed as a selective dopamine sensor.

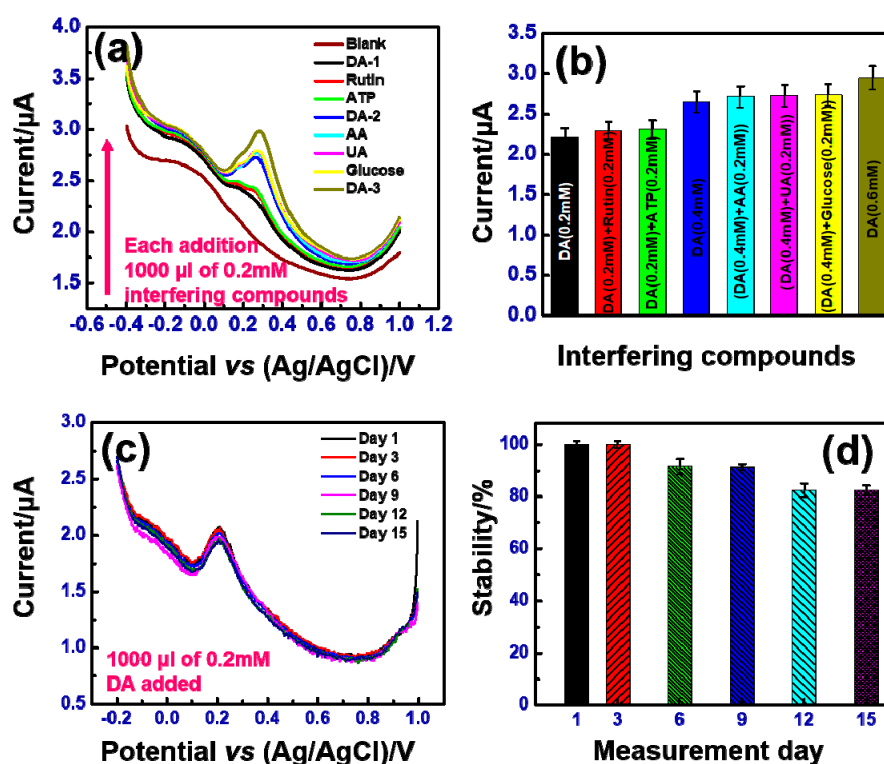


Figure 8. (a) Interference analysis of the CeO_2 /siloxene-modified electrode in the presence of other interfering compounds; (b) Current change response to the interfering compounds; (c,d) Stability of the CeO_2 /siloxene-modified electrode in the presence of 1000 μL of 0.2 mM of DA containing 0.1 M PBS solution.

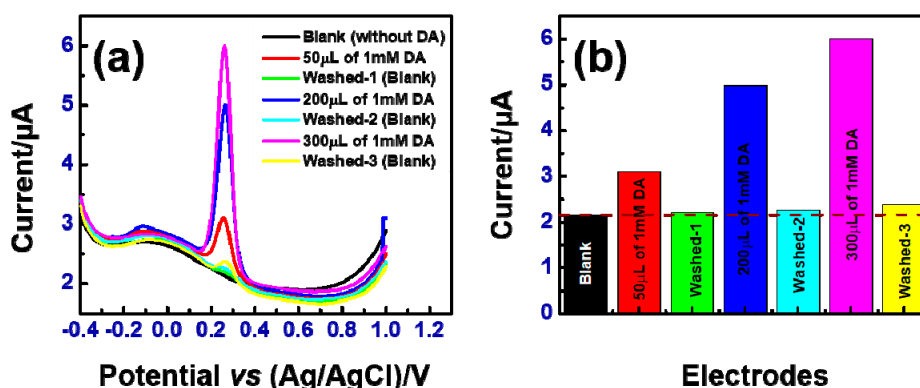


Figure 9. (a) DPV response of the CeO₂/siloxene modified electrode before and after washing in blank and DA containing PBS solutions; (b) Current changes bar chart before and after washed the electrodes.

4. Conclusions

In this work, we successfully combined Ce-MOF with siloxene and g-C₃N₄ and prepared CeO₂/siloxene and CeO₂/g-C₃N₄ composites using the pyrolysis method. The as-prepared samples were characterized by different tools and optimized the pyrolysis condition for better crystallization of CeO₂. Compared with pure CeO₂ and CeO₂/g-C₃N₄-modified electrodes, the CeO₂/siloxene-modified GCE exhibited superior electrochemical performance towards DA detection thanks to its strong redox mode between Ce and siloxene functional groups. The proposed sensor showed a detection limit of 0.292 μM with a linear range between 0.292 μM and 7.8 μM. Moreover, the CeO₂/siloxene-modified sensor possessed good repeatability and selectivity for DA detection. This work provides a new insight into preparing CeO₂ with siloxene from an MOF for highly electrocatalytic DA sensors and could be extended to the detection of other suitable biomolecules in the near future.

Supplementary Materials: The following are available online at <http://www.mdpi.com/1424-8220/20/17/4880/s1>, Figure S1: XRD pattern of the Ce-MOF, Figure S2: Cyclic voltammetry response of different amount of CeO₂/siloxene loading in 0.4 μM concentration DA containing 0.1 M PBS solution.

Author Contributions: C.G.: Methodology and Writing—original draft; R.R.: Conceptualization, Supervision and Writing—review & editing. F.W.: Supervision, Writing—review & editing. All authors have read and agreed to the published version of the manuscript.

Funding: This work was supported in part by the National Natural Science Foundation of China (Project No. 51950410598), in part by the Shenzhen Science and Technology Innovation Committee (Projects No. JCYJ20170412154426330), and in part by the Guangdong Natural Science Funds (Project No.: 2016A030306042 and 2018A050506001).

Conflicts of Interest: The authors declare no conflict of interest.

References

1. Wightman, R.M.; May, L.J.; Michael, A.C. Detection of dopamine dynamics in the brain. *Anal. Chem.* **1988**, *60*, 769A–793A. [[CrossRef](#)] [[PubMed](#)]
2. Cheng, M.; Zhang, X.; Wang, M.; Huang, H.; Ma, J. A facile electrochemical sensor based on well-dispersed graphene-molybdenum disulfide modified electrode for highly sensitive detection of dopamine. *J. Electroanal. Chem.* **2017**, *786*, 1–7. [[CrossRef](#)]
3. Liao, C.; Zhang, M.; Niu, L.; Zheng, Z.; Yan, F. Organic electrodes for highly sensitive and selective dopamine sensors. *J. Mater. Chem. B* **2014**, *2*, 191–200. [[CrossRef](#)] [[PubMed](#)]
4. Hui, X.; Xuan, X.; Kim, J.; Park, J. A highly flexible and selective dopamine sensor based on Pt-Au nanoparticle-modified laser-induced graphene. *Electrochim. Acta* **2019**, *328*, 135066. [[CrossRef](#)]
5. Jiao, J.; Zuo, J.; Pang, H.; Tan, L.; Chen, T.; Ma, H. A dopamine electrochemical sensor based on Pd-Pt alloy nanoparticles decorated polyoxometalate and multiwalled carbon nanotubes. *J. Electroanal. Chem.* **2018**, *827*, 103–111. [[CrossRef](#)]

6. Lin, M.; Song, P.; Zhou, G.; Zuo, X.; Aldalbahi, A.; Lou, X.; Shi, J.; Fan, C. Electrochemical detection of nucleic acids, proteins, small molecules and cells using a DNA-nanostructure-based universal biosensing platform. *Nat. Protoc.* **2016**, *11*, 1244–1263. [[CrossRef](#)]
7. Koo, K.M.; Carrascosa, L.G.; Shiddiky, M.J.; Analy, M.T. Poly(A) Extensions of miRNAs for Amplification-Free Electrochemical Detection on Screen-Printed Gold Electrodes. *Anal. Chem.* **2016**, *88*, 2000–2005. [[CrossRef](#)]
8. Haque, M.H.; Gopalan, V.; Yadav, S.; Islam, M.N.; Eftekhari, E.; Lin, Q.; Carrascosa, L.G.; Nguyen, N.T.; Lam, A.K.; Shiddiky, M.J. Detection of regional DNA methylation using DNA-graphene affinity interactions. *Biosens. Bioelectron.* **2017**, *87*, 615–621. [[CrossRef](#)]
9. Joutsa, J.; Voon, V.; Johansson, J.; Niemela, S.; Bergman, J.; Kaasinen, V. Dopaminergic function and intertemporal choice. *Transl. Psychiatry* **2015**, *5*, 491. [[CrossRef](#)]
10. Zhuang, X.; Mazzoni, P.; Kang, U.J. The role of neuroplasticity in dopaminergic therapy for Parkinson disease. *Nat. Rev. Neurol.* **2013**, *9*, 248–256. [[CrossRef](#)]
11. Ramachandran, R.; Zhao, C.; Rajkumar, M.; Rajavel, K.; Zhu, P.; Xuan, W.; Xu, Z.X.; Wang, F. Porous nickel oxide microsphere and Ti₃C₂T_x hybrid derived from metal-organic framework for battery-type supercapacitor electrode and non-enzymatic H₂O₂ sensor. *Electrochim. Acta* **2019**, *322*, 134771. [[CrossRef](#)]
12. Kong, B.; Tang, J.; Wu, Z.; Wei, J.; Wu, H.; Wang, Y.; Zheng, G.; Zhao, D. Ultralight Mesoporous Magnetic Frameworks by Interfacial Assembly of Prussian Blue Nanocubes. *Angew. Chem. Int. Ed.* **2014**, *53*, 2888–2892. [[CrossRef](#)] [[PubMed](#)]
13. Xu, X.; Zhang, Z.; Wang, X. Well-Defined Metal-Organic-Framework Hollow Nanostructures for Catalytic Reactions in Volving Gases. *Adv. Mater.* **2015**, *27*, 5365–5371. [[CrossRef](#)] [[PubMed](#)]
14. Huang, M.; Mi, K.; Zhang, J.; Liu, H.; Yu, T.; Yuan, A.; Kong, Q.; Xiong, S. MOF-Derived Bi-Metal Embedded N-Doped Carbon Polyhedral Nanocages with Enhanced Lithium Storage. *J. Mater. Chem. A* **2017**, *5*, 266–274. [[CrossRef](#)]
15. Meng, J.; Niu, C.; Xu, L.; Li, J.; Liu, X.; Wang, X.; Wu, Y.; Xu, X.; Chen, W.; Li, Q.; et al. General Oriented Formation of Carbon Nanotubes from Metal-Organic Frameworks. *J. Am. Chem. Soc.* **2017**, *139*, 8212–8221. [[CrossRef](#)]
16. Yang, Q.; Xu, Q.; Jiang, H.L. Metal-Organic Frameworks Meet Metal Nanoparticles: Synergistic Effect for Enhanced Catalysis. *Chem. Soc. Rev.* **2017**, *46*, 4774–4808. [[CrossRef](#)]
17. Han, L.; Yu, X.Y.; Lou, X.W. Formation of Prussian-Blue-Analog Nanocages via a Direct Etching Method and Their Conversion into Ni-Co-Mixed Oxide for Enhanced Oxygen Evolution. *Adv. Mater.* **2016**, *28*, 4601–4605. [[CrossRef](#)]
18. Ji, W.; Xu, Z.; Liu, P.; Zhang, S.; Zhou, W.; Li, H.; Zhang, T.; Li, L.; Lu, X.; Wu, J.; et al. Metal-Organic Framework Derivatives for Improving the Catalytic Activity of the CO Oxidation Reaction. *ACS Appl. Mater. Interfaces* **2017**, *9*, 15394–15398. [[CrossRef](#)]
19. Liu, H.; Zhang, S.; Liu, Y.; Yang, Z.; Feng, X.; Lu, X.; Huo, F. Well-Dispersed and Size-Controlled Supported Metal Oxide Nano-particles Derived from MOF Composites and Further Application in Catalysis. *Small* **2015**, *11*, 3130–3134. [[CrossRef](#)]
20. Chen, T.; Liu, X.; Niu, L.; Gong, Y.; Li, C.; Xu, S.; Pan, L. Recent progress on metal-organic framework-derived materials for sodium-ion battery anodes. *Inorg. Chem. Front.* **2020**, *3*, 567–582. [[CrossRef](#)]
21. Guo, Z.; Song, L.; Xu, T.; Gao, D.; Li, C.; Hu, X.; Chen, G. CeO₂-CuO bimetal oxides derived from Ce-based MOF and their difference in catalytic activities for CO oxidation. *Mater. Chem. Phys.* **2019**, *26*, 338–343. [[CrossRef](#)]
22. Xie, X.; Huang, K.; Wu, X. Metal-organic framework derived hollow materials for electrochemical energy storage. *J. Mater. Chem. A* **2017**, *7*, 6754–6771. [[CrossRef](#)]
23. Zhang, S.; Gao, H.; Xu, X.; Cao, R.; Yang, H.; Xu, X.; Li, J. MOF-derived CoN/N-C@SiO₂ yolk-shell nanoreactor with dual active sites for highly efficient catalytic advanced oxidation processes. *Chem. Eng. J.* **2020**, *381*, 122670. [[CrossRef](#)]
24. Phoka, S.; Laokul, P.; Swatsitang, E.; Promarak, V.; Seraphin, S.; Maensiri, S. Synthesis, structural and optical properties of CeO₂ nanoparticles synthesized by a simple polyvinyl pyrrolidone (PVP) solution route. *Mater. Chem. Phys.* **2019**, *115*, 423–428. [[CrossRef](#)]
25. Dhall, A.; Self, W. Cerium oxide nanoparticles: A brief review of their synthesis methods and biomedical applications. *Antioxidants* **2018**, *7*, 97. [[CrossRef](#)] [[PubMed](#)]

26. Goharshadi, E.K.; Samiee, S.; Nancarrow, P. Fabrication of cerium oxide nanoparticles: Characterizations and optical properties. *J. Colloid Interface Sci.* **2011**, *356*, 473–480. [[CrossRef](#)] [[PubMed](#)]
27. Ramachandran, R.; Len, X.; Zhao, C.; Xu, Z.; Wang, F. 2D siloxene sheets: A novel electrochemical sensor for selective dopamine detection. *Appl. Mater. Today* **2019**, *18*, 100477. [[CrossRef](#)]
28. Zhang, Y.L.; Li, B.; Guan, W.; Wei, Y.N.; Yan, C.H.; Meng, M.J.; Pan, J.M.; Yan, Y.S. One-pot synthesis of HMF from carbohydrates over acid-base bi-functional carbonaceous catalyst supported on halloysite nanotubes. *Cellulose* **2020**, *27*, 3037–3054. [[CrossRef](#)]
29. Zhu, Z.; Huo, P.W.; Lu, Z.Y.; Yan, Y.S.; Liu, Z.; Shi, W.D.; Li, C.X.; Dong, H.J. Fabrication of magnetically recoverable photocatalysts using g-C₃N₄ for effective separation of charge carriers through like-Z-scheme mechanism with Fe₃O₄ mediator. *Chem. Eng. J.* **2018**, *331*, 615–625. [[CrossRef](#)]
30. Hu, S.; Ma, L.; You, J.; Li, F.; Fan, Z.; Lu, G.; Liu, D.; Gui, J. Enhanced visible light photocatalytic performance of g-C₃N₄ photocatalysts Co-doped with iron and phosphorus. *Appl. Surf. Sci.* **2014**, *311*, 164–171. [[CrossRef](#)]
31. Oh, W.D.; Chang, V.W.C.; Hu, Z.T.; Goei, R.; Lim, T.T. Enhancing the catalytic activity of g-C₃N₄ through Me doping (Me = Cu, Co and Fe) for selective sulfathiazole degradation via redox-based advanced oxidation process. *Chem. Eng. J.* **2017**, *323*, 260–269. [[CrossRef](#)]
32. Mo, Z.; She, X.; Li, Y.; Liu, L.; Huang, L.; Chen, Z.; Zhang, Q.; Xu, H.; Li, H. Synthesis of g-C₃N₄ at different temperatures for superior visible/UV photocatalytic performance and photoelectrochemical sensing of MB solution. *RSC Adv.* **2015**, *5*, 101552–101562. [[CrossRef](#)]
33. Zou, J.; Wu, S.; Liu, Y.; Sun, Y.; Cao, Y.; Hsu, J.; Wee, A.; Jiang, J. An ultrasensitive electrochemical sensor based on 2D g-C₃N₄/CuO nanocomposites for dopamine detection. *Carbon* **2018**, *130*, 652–663. [[CrossRef](#)]
34. Xavier, M.; Nair, P.; Mathew, S. Emerging trends in sensors based on carbon nitride materials. *Analyst* **2019**, *144*, 1475–1491. [[CrossRef](#)] [[PubMed](#)]
35. Sakthivel, T.; Ramachandran, R.; Kirubakaran, K. Photocatalytic properties of copper-two dimensional graphitic carbon nitride hybrid film synthesized by pyrolysis method. *J. Environ. Chem. Eng.* **2018**, *6*, 2636–2642. [[CrossRef](#)]
36. Ramachandran, R.; Xuan, W.; Zhao, C.; Len, X.; Sun, D.; Luo, D.; Wang, F. Enhanced electrochemical properties of cerium metal–organic framework based composite electrodes for high-performance supercapacitor application. *RSC Adv.* **2018**, *8*, 3462–3469. [[CrossRef](#)]
37. Chen, X.; Yu, E.; Cai, S.; Jia, H.; Chen, J.; Liang, P. In situ pyrolysis of Ce-MOF to prepare CeO₂ catalyst with obviously improved catalytic performance for toluene combustion. *Chem. Eng. J.* **2018**, *334*, 469–479. [[CrossRef](#)]
38. Rajkumar, C.; Thirumalraj, B.; Chen, S.-M.; Chen, H.-A. A simple preparation of graphite/gelatin composite for electrochemical detection of dopamine. *J. Colloid Interface Sci.* **2017**, *487*, 149–155. [[CrossRef](#)]
39. Saenz, H.S.C.; Saravia, L.P.H.; Selva, J.S.G.; Sukeri, A.; Montero, P.J.E.; Bertotti, M. Electrochemical dopamine sensor using a nanoporous gold microelectrode: A proof-of-concept study for the detection of dopamine release by scanning electrochemical microscopy. *Microchim. Acta* **2018**, *185*, 367. [[CrossRef](#)]
40. Sukanya, R.; Ramki, S.; Chen, S.-M.; Karthik, R. Ultrasound treated cerium oxide/tin oxide (CeO₂/SnO₂) nanocatalyst: A feasible approach and enhanced electrode material for sensing of anti-inflammatory drug 5-aminosalicylic acid in biological samples. *Anal. Chim. Acta* **2020**, *1096*, 76–88. [[CrossRef](#)]
41. Sakthivel, R.; Kubendhiran, S.; Chen, S.-M. One-pot sonochemical synthesis of marigold flower-like structured ruthenium doped bismuth sulfide for the highly sensitive detection of antipsychotic drug thioridazine in the human serum sample. *J. Taiwan Inst. Chem. Eng.* **2020**, *111*, 270–282. [[CrossRef](#)]
42. Vali, A.; Malayeri, H.Z.; Azizi, M.; Choi, H. DPV-assisted understanding of TiO₂ photocatalytic decomposition of aspirin by identifying the role of produced reactive species. *Appl. Catal. B Environ.* **2020**, *266*, 118646. [[CrossRef](#)]
43. Moccellini, S.; Fernandes, S.; Vieira, I. Bean sprout peroxidase biosensor based on l-cysteine self-assembled monolayer for the determination of dopamine. *Sens. Actuators B Chem.* **2018**, *133*, 364–369. [[CrossRef](#)]
44. Roychoudhury, A.; Basu, S.; Jha, S. Dopamine biosensor based on surface functionalized nanostructured nickel oxide platform. *Biosens. Bioelectron.* **2016**, *84*, 72–81. [[CrossRef](#)]
45. Dervisevic, M.; Senel, M.; Cevik, E. Novel impedimetric dopamine biosensor based on boronic acid functional polythiophene modified electrodes. *Mater. Sci. Eng. C* **2017**, *72*, 641–649. [[CrossRef](#)]
46. Chandra, S.; Arora, K.; Bahadur, D. Impedimetric biosensor based on magnetic nanoparticles for electrochemical detection of dopamine. *Mater. Sci. Eng. B* **2012**, *177*, 1531–1537. [[CrossRef](#)]

47. How, G.T.S.; Pandikumar, A.; Ming, H.N.; Ngee, L.H. Highly exposed {001} faces of titanium dioxide modified with reduced graphene oxide for dopamine sensing. *Sci. Rep.* **2014**, *4*, 5044.
48. Mani, V.; Devasenathipathy, R.; Chen, S.-M.; Kohilarani, K.; Ramachandran, R. A sensitive amperometric sensor for the determination of dopamine at graphene and bismuth nanocomposite film modified electrode. *Int. J. Electrochem. Sci.* **2015**, *10*, 1199–1207.



© 2020 by the authors. Licensee MDPI, Basel, Switzerland. This article is an open access article distributed under the terms and conditions of the Creative Commons Attribution (CC BY) license (<http://creativecommons.org/licenses/by/4.0/>).